ELSEVIER

Nuclear Physics A 620 (1997) 127–150

NUCLEAR PHYSICS A

Study of ^{113}Cd by the ^{110}Pd(α,nγ) reaction ★

N. Warr [a], S. Drissi [a], P.E. Garrett [b], J. Jolie [a], J. Kern [a], S.J. Mannanal [a], J.-L. Schenker [a], J.-P. Vorlet [a]

[a] *Physics Department, University, CH-1700 Fribourg, Switzerland*

[b] *Dept. of Physics and Astronomy, University of Kentucky, Lexington, KY 40506, USA*

Received 25 October 1996

Abstract

The nuclear structure of ^{113}Cd was studied using in-beam γ-ray spectroscopy. A level scheme, consisting of 65 levels and more than 100 transitions, was constructed on the basis of $\gamma\gamma$ coincidences using five compton-suppressed Ge detectors. Spins were assigned by means of excitation function slopes and angular distribution analysis. The resulting level scheme was interpreted in the framework of the interacting boson–fermion model. © 1997 Elsevier Science B.V.

PACS: 23.20.Lv; 23.20.En; 27.60.+j; 21.60.Fw; 29.30.Kv

Keywords: NUCLEAR REACTION: ^{110}Pd(α,nγ), E = 12.2, 14.9, 16.2, 18.0 MeV; Measured E_γ, $I_\gamma(\theta)$, $\gamma\gamma$-coin. ^{113}Cd deduced levels, J, π. Comparison with interacting boson–fermion model. Enriched targets; Compton-suppressed Ge detectors

1. Introduction

The ^{113}Cd nucleus plays an important rôle in the understanding of nuclear synthesis. Once it is formed by the β-decay of ^{113}Ag, it may either decay to the quasi-stable ground state or to the $\frac{11}{2}^-$ isomer at 263 keV, which has a half-life of 14 years. The large thermal neutron capture cross-section of the ground state favours the s-process in the neutron flux of the stellar environment. The $\frac{11}{2}^-$ isomer, on the other hand, will tend to β-decay. Thus there are two separate reaction chains. The synthesis of nearby isotopes is dependent on the relative populations of the ground-state and the isomer, which are also influenced by (γ,γ') excitations occurring in supernovæ. The (γ,γ') process leading to the population of the $\frac{11}{2}^-$ isomer is an indirect one, proceeding

★ Work supported in part by the Swiss National Science Foundation and by PSI/Villigen.

PII S0375-9474(97)00165-6

through many excited states, and can be understood only if a detailed knowledge of the level structure of ^{113}Cd is available. It is therefore important for astrophysicists to obtain information about the structure of ^{113}Cd because of its influence on the relative abundances of the isotopes in this mass region [1].

The nuclear structure of ^{113}Cd also provides a good test of the interacting boson fermion model (IBFM), since the even–even core ^{112}Cd is well described by the $U(5)$ limit of the IBM [2,3]. This means it is possible to perform IBFM calculations varying only the parameters describing the odd neutron and its coupling to the even–even core. These parameters may be further restricted by considering semi-microscopic arguments. Of particular interest is the search for intruder states, which have been observed [4] in the adjacent even–even nuclei, in the odd-A nuclei in this region near a semi-closed shell.

In Section 2, the experiments performed to study the ^{113}Cd nucleus and their results will be described. In Section 3, the level scheme determined from these results will be presented and in Section 4, individual levels will be discussed. Finally, in Section 5, the level scheme will be compared with theoretical calculations in the framework of the IBFM.

2. Experimental procedure

In the experiments of the present work, the ^{113}Cd nuclei were produced by the ^{110}Pd(α,nγ) reaction using alpha particles accelerated in the Philips variable-energy cyclotron at the Paul Scherrer Institute (PSI) in Villigen, Switzerland. A self-supporting 10 mg/cm^2 foil enriched to 98.9% in ^{110}Pd was used as the target for all experiments.

2.1. Excitation functions

Two intrinsic Ge detectors having volumes of 65 and 83 cm^3, equipped with BGO–NaI(Tl) Compton suppression shields, were used to record γ-ray spectra at beam energies of 12.2, 14.9, and 18.0 MeV. Radioactive sources of ^{133}Ba and ^{152}Eu were used for energy and efficiency calibrations of the detectors. The γ-ray energies were calibrated by measuring simultaneously the in-beam reaction and calibration sources. The smaller volume detector, which had a resolution of about 1 keV FWHM at 122 keV, was used to measure spectra up to about 900 keV, whereas the larger detector, which had a resolution of 1.8 keV at 1 MeV, was used to measure up to 2.5 MeV.

At low beam energies, the cross-section for compound nucleus formation is greatly reduced by the Coulomb barrier. As a result, the cross-section for the (α,2n) reaction is much greater than for the (α,n) channel at their respective maxima. Furthermore, the two channels are about equal in strength at the beam energy corresponding to the maximum of the (α,n) channel. It is necessary, therefore, to work at a lower energy in order to prevent the domination of the (α, 2n) channel. The determination of the optimum energy to favour ^{113}Cd production is crucial and a compromise must be

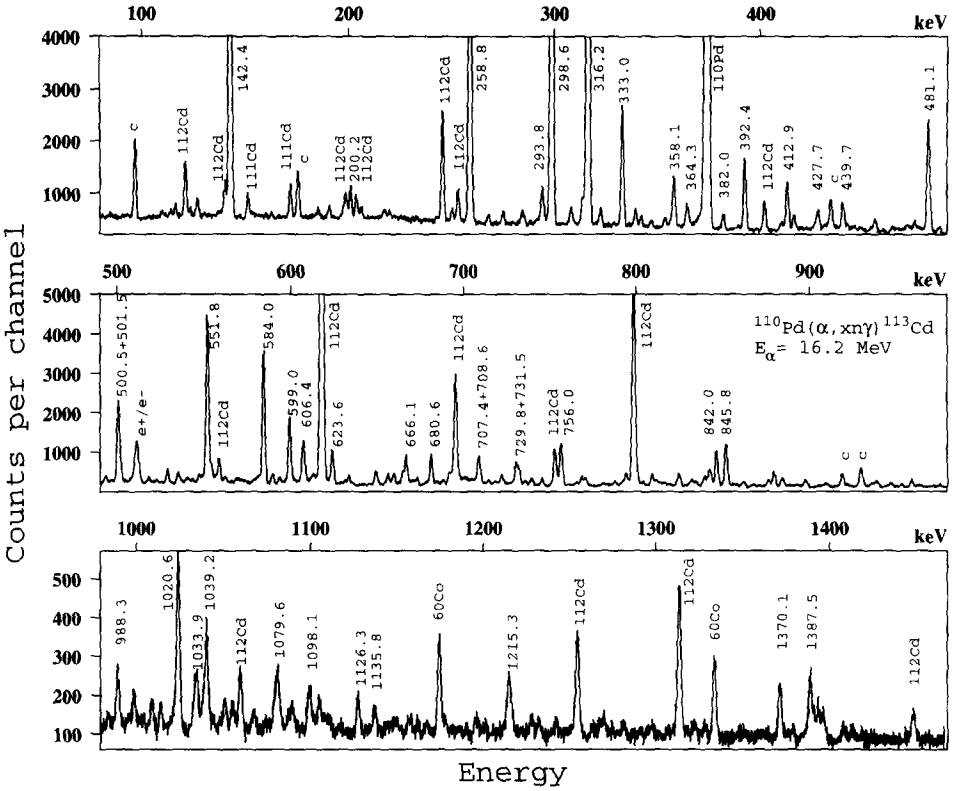

Fig. 1. Part of a spectrum of the reaction ^{110}Pd(α,xnγ) at 16 MeV beam energy. The ^{113}Cd γ-rays are labelled by their energies. Transitions from other known nuclei are labelled by the name of the isotope and those from contaminants are denoted 'c'.

obtained between favouring the absolute cross-section for the desired reaction channel, and the relative cross-section with respect to the competing channel. This optimum was found to be at approximately 16 MeV and all subsequent measurements were performed at 16.2 MeV. At this energy, the main contributions to the spectra are from the (α,n) and the (α,2n) channels and the Coulomb excitation of the ^{110}Pd target (see Fig. 1). Production of ^{111}Cd by the (α,3n) reaction is not observed at this beam-energy because of the Q-value; however, a small amount of ^{111}Cd is produced by the (α,n) reaction on ^{108}Pd, the main target impurity.

The form of the excitation functions were used to assign the observed γ-rays to a particular nucleus and the slopes of the excitation functions provided an indication of the spins of levels in ^{113}Cd (see Section 3.1.2).

2.2. *Angular distributions*

A Compton-suppression spectrometer [5], using the above mentioned 83 cm^3 detector, was used to record γ-ray spectra at eight angles between 30° and 90° with respect to the beam direction, at a distance of about 80 cm from the target. The system was

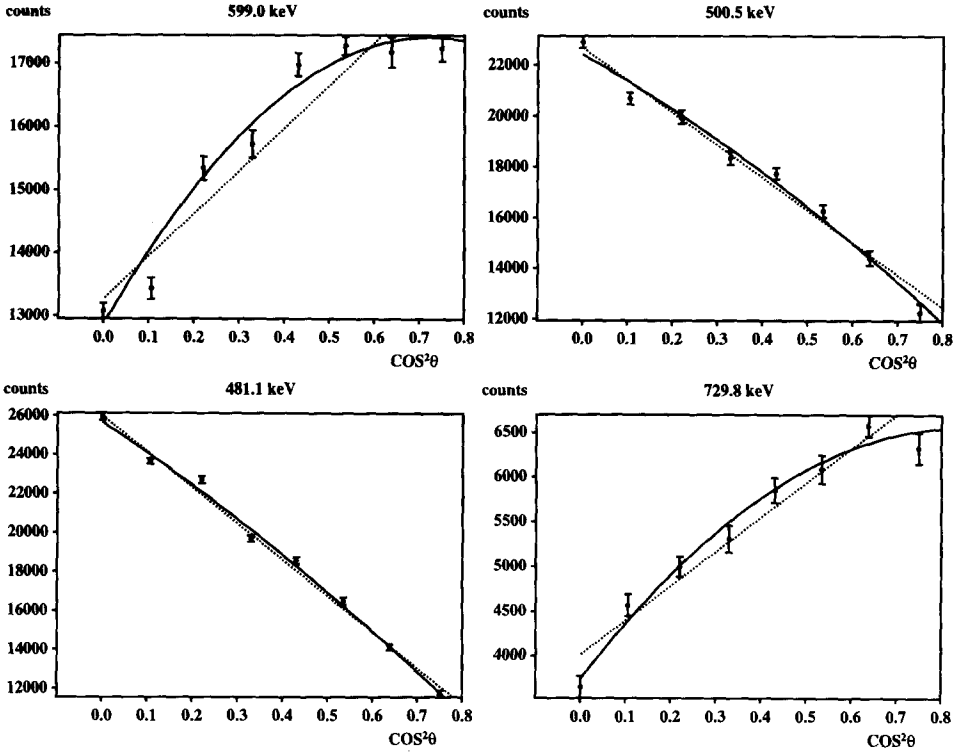

Fig. 2. Angular distributions of selected γ-rays. The dotted lines are fits with only a second order Legendre polynomial, whereas the solid curves are with a fourth order polynomial.

corrected for anisotropy, which was found to be of the order of 0.5%, by measuring with radioactive sources placed precisely at the target position. Fluctuations in beam intensity were corrected for by normalising to the X-rays observed by a fixed monitor detector. Dead-time corrections were performed for both detectors by comparing the number of ADC conversions with counters which recorded the number of events entering the ADCs for each detector. Correction for solid-angle effects was unnecessary since the angle subtended by the target at the detector was small.

The normalised peak areas were fitted as a function of angle with a fourth order even Legendre polynomial in order to determine the coefficients $A_0(=I_\gamma)$, A_2/A_0 and A_4/A_0, which are shown in Table 1, which also reports the γ-ray energies together with their statistical errors. Fig. 2 illustrates the angular distributions of selected γ-rays.

2.3. $\gamma\gamma$-coincidences

Initially, the system of three Ge detectors described in Ref. [3] was used to measure $\gamma\gamma$-coincidences for ^{113}Cd. Due to the relatively low cross-section for the (α,n) channel compared with the (α,2n) channel, this resulted in a very low count rate in the (α,n) channel. To resolve this problem a system of five intrinsic Ge detectors equipped with BGO–NaI(Tl) Compton shields was developed (see Fig. 3), whose mean target-detector

Table 1
Summary of the results of the angular distribution and excitation function experiments

E_γ [keV]	A_0	A_2/A_0	A_4/A_0	Mul.	δ	$E_{initial}$	Slope
115.96(2)	6.0(9)	0.08(5)		DP		638.4	13(8)
126.48(1)	8.6(8)	0.14(4)	−0.07(5)	E2		1177.8	−22(3)
142.42(1)	540(100)	−0.24(2)		DP	−0.020(2)	458.6	8.3(3)
153.0(1)	1.2(5)					1367.5	
184.83(2)	4.5(6)					1124.7	
205.93(2) [a]	6.4(7)					522.5	−9(9)
217.08(2)	4.7(5)					855.4	−20(10)
231.0(1)	1.0(4)					1047.7	
237.75(8)	1.8(5)					1896.7	
238.96(9)	1.4(6)					1896.7	
242.64(4)	2.5(4)	−0.3(2)				1126.2	
249.95(2)	7.4(5)	−0.2(1)		DP		708.6	−1(7)
258.77(1)	493(8)	0.12(2)	−0.02(3)			522.5	−2.8(9)
267.77(2)	7.5(5)	0.28(5)			0.10(4)	584.0	−9(8)
274.89(2)	9.8(5)	−0.38(6)		DP	−0.02(1)	1214.7	
285.3(1)	4(1)					584.0	−2(2)
293.79(7)	30(1)	0.2(1)				1109.5	29(7)
298.60(1)	860(11)	0.05(2)		DP	0.40(1)	298.6	−8.4(2)
307.89(2)	13.6(7)	−0.61(7)		DP		1124.7	
313.48(1)	18.3(6)	−0.11(6)		DP	0.41(2)	897.5	19(6)
313.48(1)	18.3(6)	−0.11(6)		DP	0.6(1)	897.5	19(6)
316.22(1)	1000(10)	0.25(2)	−0.04(3)	E2		316.2	0.00(2)
322.36(2)	15.8(6)	0.1(1)				1177.8	−15(4)
332.99(1)	111(2)	0.15(2)		DP	−0.21(7)	855.4	−12.6(6)
335.98(9)	1.4(6)					1513.9	
339.33(1)	16.9(8)					1194.8	−41(2)
358.09(1)	50(1)	0.27(2)		DP	0.003(3)	816.7	
364.31(6)	17(8)					680.6	−18(3)
365.4(2)	6(9)					1733.0	
370.26(3)	12(2)					1051.3	
374.72(1)	48(2)	0.273(84)				638.4	22(6)
381.95(2)	16.1(6)	0.07(2)		DP	0.02(1)	680.6	−30(3)
381.95(2)	16.1(6)	0.07(2)		DP	4.7(2)	680.6	−30(3)
392.36(1)	72(1)	0.15(1)		DP	−0.05(2)	708.6	−12(1)
410.11(5)	8.7(6)	−0.20(8)		DP	−0.08(4)	708.6	−30(20)
412.90(1)	57(1)	0.13(2)	−0.05(3)	E2		1051.3	−1(2)
416.09(1)	17.0(7)	0.23(5)	−0.18(7)	E2		1124.7	−5(4)
427.71(2)	20(1)	−0.49(6)		DP		1367.5	20(10)
439.74(4)	33(1)					897.5	
444.95(4) [a]	3.4(7)					1261.9	
453.4(1)	4.3(7)					1037.4	
463.84(4)	7(1)	−0.6(1)		DP	−0.02(3)	1047.7	
469.5(2)	0.6(8)					1367.5	
471.20(8)	5.4(9)	0.4(2)	−0.3(3)	E2		1109.5	
481.13(1)	153(2)	−0.62(2)		DP	−0.04(5)	939.8	18(2)
500.50(1)	147(3)	−0.46(3)		DP	0.04(5)	816.7	7(2)
501.77(2)	35(2)	0.57(4)		DP	0.00(3)	1626.5	
518.15(3)	9.1(7)	−0.34(8)		DP		1733.0	15(16)
528.81(1)	27.8(9)	0.39(3)		DP		1051.3	0(3)

Table 1 — continued

E_γ [keV]	A_0	A_2/A_0	A_4/A_0	Mul.	δ	E_{initial}	Slope
534.87(3)	20(1)	0.45(4)		DP	0.00(5)	1902.4	19(9)
539.3(1)	3(1)	−0.2(2)		E1	−0.004(3)	855.4	
540.78(6)	6(1)					999.4	
543.20(5)	3(1)					1181.5	
550.86(4)	40(6)	0.2(1)		DP	−0.006(7)	1367.5	
551.79(1)	343(8)	0.50(3)	−0.10(4)	E2		815.5	46(1)
553.90(1)	35(2)	0.56(3)		DP	0.0(1)	1192.4	30(7)
561.56(9)	9.1(9)					1671.0	14(23)
579.8(1)	6(1)					878.4	
581.26(9)	13(6)					897.5	
583.97(1)	301(3)	0.24(2)	−0.05(3)	E2		584.0	−11.4(4)
589.02(2)	19(1)	0.3(1)		DP	0.005(10)	1047.7	−11(4)
593.23(2)	11(1)	0.3(2)	−0.3(2)	E2		2219.7	
598.95(1)	147(2)	0.23(5)	−0.15(6)	E2		897.5	4(1)
606.39(6)	4(1)	−1.0(1)		DP		1461.8	44(6)
621.5(2)	8(2)					1561.7	
623.58(2)	77(2)					939.8	19(2)
633.08(2)	22(2)	0.1(1)	−0.4(2)	(E2)		2147.0	26(8)
655.48(1)	26(1)	−0.21(5)		DP	−0.001(2)	1177.8	−18(3)
659.08(3)	27(2)	0.43(8)				1181.5	21(3)
664.13(2)	32(1)	0.36(9)	−0.4(1)	E2		1561.7	30(4)
666.12(1) [a]	71(2) [b]					1124.7	
670.20(5) [a]	13(1)					1192.4	−3(6)
672.34(2)	17(1)					1194.8	−28(4)
677.95(4)	7.1(9)					1261.9	
680.64(1) [a]	78(2)	−0.13(5)		DP	−1.34(5)	680.6	−22(1)
680.64(1) [a]	78(2)	−0.13(5)		DP	−0.13(2)	680.6	−22(1)
687.6(1)	12(1)					1902.4	−14(9)
691.23(6)	25(2)					1007.5	
696.5(2) [a]	<1.0					1405.6	
707.44(4)	24(4)					1647.2	3(1)
708.58(2)	62(5)					708.6	−4(4)
713.91(5)	9(1)	−0.42(6)		DP	−0.01(2)	1823.4	
721.24(4)	22(1)	0.7(6)		DP		1037.4	−12(4)
729.79(2)	58(2)	0.43(4)	−0.17(6)	E2		1313.8	19(3)
731.47(2)	45(2)	−0.52(4)		DP	−0.03(4)	1047.7	6(4)
735.20(2)	12.6(9)					1033.8	−11(5)
738.84(1)	21(1)	0.40(3)	−0.03(5)		1.1(5)	1037.4	−14(6)
743.6(4)	<3					1327.6	
744.99(2)	19(1)	0.16(3)				1561.7	3(3)
756.03(1)	140(4)	0.34(4)	−0.19(5)	E2		1214.7	32(1)
765.15(1)	7.4(9)	0.6(1)		DP		1620.6	
770.50(6)	14(4)					1451.1	20(6)
787.12(2)	13(1)	0.3(2)	−0.5(3)	(E2)		1896.7	
793.40(4) [a]	28(2)	0.4(2)	−0.5(4)			1733.0	2(6)
799.57(8)	48(5)	0.5(2)		DP		1321.6	12(7)
803.23(5)	9(1)	−0.5(1)		DP		1261.9	−8(4)
808.48(2)	29(2)	0.40(5)	−0.19(8)	E2		1124.7	9(4)
824.27(3)	31(4)	0.4(1)	−0.2(2)	E2		1346.7	7(5)
831.55(6)	18(2)	0.25(5)	−0.13(7)	E2		2046.6	

Table 1 — continued

E_γ [keV]	A_0	A_2/A_0	A_4/A_0	Mul.	δ	$E_{initial}$	Slope
842.06(3)	53(2)	0.36(8)	−0.3(1)	E2		1657.6	11(5)
845.78(1)	125(2)	0.64(3)		DP		1109.5	33(2)
855.10(6)	4(1)					1313.8	
875.54(3)	18.1(9)	0.2(1)	−0.2(2)	E2		1513.9	11(7)
878.4(2)	4(1)					878.4	−24(1)
879.2(3)	2(2)					1177.9	
883.43(4)	29(1)	−1(1)				1405.6	
892.12(5)	6(1)					1190.8	−8(13)
896.62(4)	22(2)					1195.2	−1(5)
906.0(2)	3.3(9)					1364.7	
909.5(5)	6(4)					1367.5	
920.94(3)	9.0(9)	−0.4(1)		DP		1504.9	
929.4(2) [a]	5(1)					1513.9	
931.9(3)	5(1)					1871.7	
937.19(3)	19(2)					1396.0	
946.01(6) [a]	6(3)					1261.9	
949.8(1)	2.4(8)					2164.5	
952.04(5)	10(1)					1410.7	
969.59(5)	5.8(8)					1268.3	
988.29(3)	24(1)					988.3	
1007.90(3)	14(1)	0.1(2)	−0.2(2)			1823.4	
1020.64(6) [a]	8(1)	−0.2(2)				1658.4	
1033.9(5)	12(1)	−0.2(1)				1033.8	
1037.18(5) [a]	12(1)					1037.4	
1049.7(1)	12.4(1)					1049.7	
1066.11(7)	9.1(1)	−0.38(7)		DP		1364.7	
1079.63(4)	26(2)	0.2(1)	−0.4(2)			1396.0	
1081.38(9)	8(2)					1896.7	
1088.63(8)	12(1)					1904.1	
1098.06(7)	17(2)	0.3(2)	−0.1(3)			1620.6	
1107.1(1)	8.0(9)					1405.6	
1126.28(4)	18(1)					1126.2	
1135.80(4)	11(1)	−0.6(2)				1658.4	
1215.27(6)	14(2)					1737.7	
1221.3(2)	2.9(9)					1743.7	
1226.71(5)	10(1)	0.6(1)	−0.1(2)			2042.2	
1268.48(5) [a]	10(1)					1268.3	
1279.84(6)	6(1)					1279.8	
1370.08(5)	34(1)	0.42(9)	−0.2(1)			1892.5	
1387.50(4)	34(2)					1387.5	
1394.8(1)	14(2)					1658.4	

[a] γ-ray placed by coincidence relations for which the energy does not satisfy the Ritz condition due to the influence of neighbouring peaks.

[b] The 666.1 keV transition is not resolved from a transition in ^{112}Cd. The quoted A_0 value should, therefore, be treated as an upper limit.

distance was 15 cm. As can be seen from Fig. 3, the upper BGO–NaI(Tl) shields two Ge detectors, with no heavy metal shielding between them. As a result, scattering between this pair of Ge detectors is possible, producing spurious events. Such events are eliminated by a further on-line anti-coincidence condition between the detectors in the

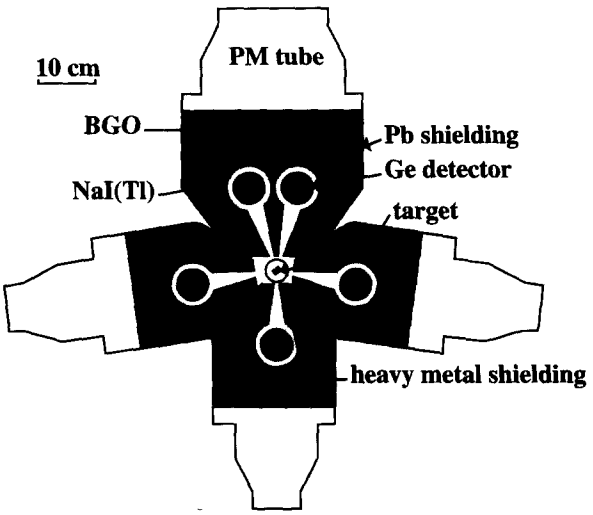

Fig. 3. Experimental arrangement of five Ge detectors with BGO–NaI(Tl) Compton shields.

upper Compton shield. Note that with this arrangement a rather compact system could be achieved.

The five intrinsic Ge detectors had volumes ranging from 65 to 115 cm^3 with an average of 95 cm^3. Times (T_{i-RF}) relative to the radio frequency of the accelerator along with the energy (E_i) for each detector were recorded on-line whenever the electronics registered events coincident within about 150 ns. The data were recorded in list-mode, and a coincidence matrix was constructed off-line, where more stringent conditions on the T_{i-RF} and ($T_{i-RF} - T_{j-RF}$) time differences were applied.

With a beam current of about 10 nA just over 200 valid coincidences per second were obtained compared with only 30 per second for the three-detector setup [3]. In total 10^8 events were recorded of which 2.2×10^7 satisfied the rather stringent off-line sorting conditions. Table 2 lists results of selected coincidence gates, and Fig. 4 shows coincidence spectra of a few important gates.

3. Construction of level scheme

Several criteria were used to establish the level scheme, the most important being from the coincidence measurement. In most cases, the coincidence relations allow the unambiguous placement of γ-rays. A small number of γ-rays were placed on the basis of the Ritz combination principle provided that the excitation function slopes [6] were compatible with those of other γ-rays depopulating the same level. No levels were established without confirmation from the coincidence measurement. The level scheme established in this work is presented in Figs. 5–8. Note that the energy scale is non-linear.

Table 2
Qualitative summary of the coincidence measurement results

Gate [keV]	Display[a] [keV]
142	203 243 250* 275* **299*** 308* **316*** **358*** 374[c] 428* 433 440[w]* **481*** **501*** **518*** 535* 541* 551* (589)* (593) **666*** 688* **707*** **756*** **793*** 803* **832*** (855)* (869) 883 (897) 910* 939* 950 952* (1202) (1242) (1265)
259	116* 203 322* **333*** 339* 374[c] **529*** **606*** **655*** **659*** **670*** **672*** 756 765 **800*** **824*** 883* 1098* 1136* (1215)* (1221)* (1328) (1368) (1370)*
275	**142*** **299*** **316*** **481*** 624*
299	**142*** 275* 285* 308* 358* 364* 374[c] 382* 392* 410* 416* 428* (431) 440* (469)* **481*** **500*** 518* 535* 580[w]* 599* 624* 666* 688* 691* 707* 731* 735* 739* 756* 793* 803* 808* 879* (883) 892* 897* 1066* (1281)
308	**142*** **299*** **316*** **358*** 374[c] **500*** 554 617[c] (897)
313	**584*** 664*
316	**142*** (206)* (250)* 268* 275* **308*** **358*** 364* 374[c] **392*** **416*** **428*** **440*** **481*** 493 **500*** 535* 539* 551* 581* **624*** **666*** 685[w] 691 **707*** 721* **731*** (745)* **756*** 793* 808* 832* 1080*
322	**259*** **333*** 336* 374[c] (539)
333	**259*** **322*** **339*** **606*** (624) 765
339	**259*** **333*** (697)
358	**142*** **299*** **308*** **316*** (502)* 551*
375	(217)* 374[c] **413*** **440[c]** 543* 547[c] **554*** **648** **707** 768 824 **839[c]** 1034 1098
392	**299*** **316*** 374[c] 416* 502* 697*
413	**375***
416	(250)* 299* 316* **392***
428	**142*** **299*** **316*** (365)* **481*** 535* 624*
481	**142*** 185* **275*** **299*** **316*** 336 365* **428*** 535* 622* 629 **707*** (727) **793*** (897) (929)
500	**299*** **308*** **316*** 445 502* 535* **551*** 613 745* 752[c] 940
502	**142*** **299*** **308*** **316*** (374[c]) (392)* (416)* 500* **666*** 798[c] 808*
518	**142*** **299*** **316*** **756***
529	**259***
552	**294*** **842*** 1008* 1081* 1089* 1224 1227*
581	299* 316*
584	**313*** (453)* (527) (554) 556 593 617[c] 678* **730*** 743* (888) 921* 929* (1162)
599	**299*** 305 470* (535)* **664***
624	275* **316*** **428*** 707* 793*
655	**259***
678	374[c] 584*
707	**142*** **299*** **316*** **481*** 624*
721	(299)* 316*
744	(500)[c] 584*
745	299* 316* 500* 584[c]
756	**142*** (153)* **299*** **316*** 518* (541) 688* 832* 950*
824	**259*** (800)
842	**552*** (668)
846	237 562* 714* 787* 795 937 974
878	299*
883	259*
897	299*

[a] Bold print indicates a strong coincidence, brackets indicate a questionable one, a 'c' indicates a contaminating coincidence from another line and 'w' indicates that the coincident peak appears to be wide. An asterisk indicates that the coincidence relation are in accordance with the level scheme.

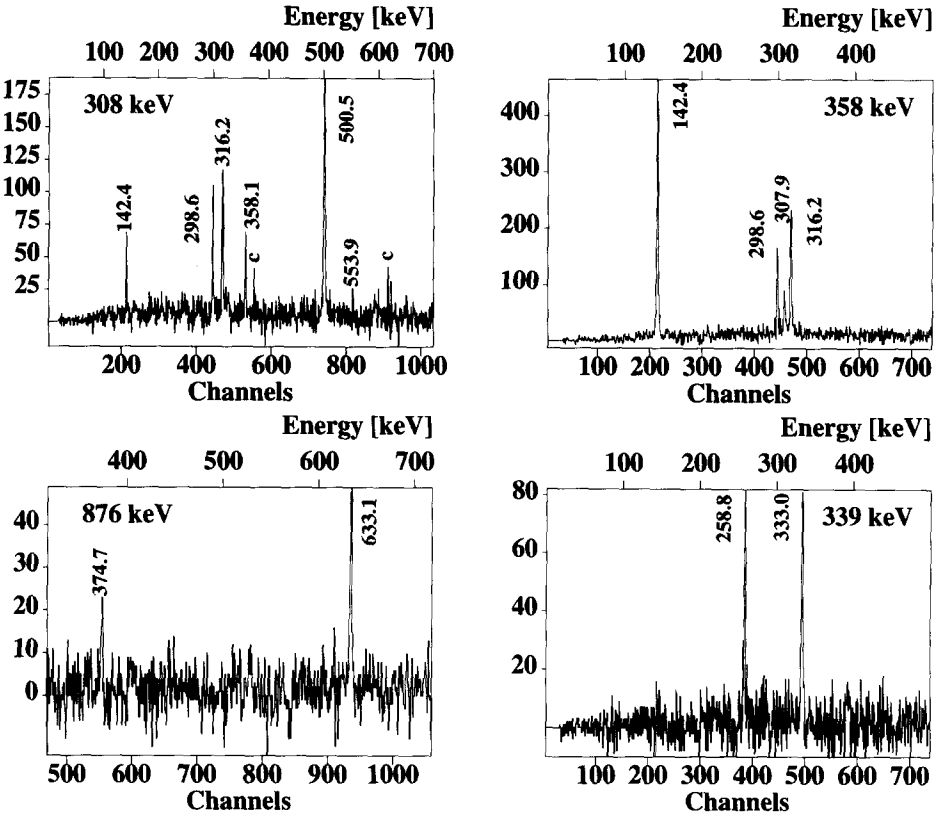

Fig. 4. Selected coincidence gates. 'c' denotes a coincidence with a line attributed to a contaminant.

3.1. Determination of spins and parities

The spins and parities of the levels may be determined by considering the γ-rays which depopulate those levels. Firstly, since only E1, M1 and E2 transitions are expected to be observable in the prompt spectra, limits may be set on possible spins on the basis of the observation of particular transitions. Furthermore, in general, three methods may be used to determine the spin of a state: (i) the analysis of the angular distributions of the γ-rays depopulating the level, (ii) the slopes of the excitation function and (iii) the side-feeding intensity. The use of side-feeding intensities was not possible in this case due to the contamination from the (α,2n) channel which may influence the side-feeding intensities. In view of the proximity of the Coulomb barrier and the large contribution to the spectra of the (α,2n) channel, many lines do not yield satisfactory angular distributions or excitation functions. Consideration of all the γ-rays depopulating a given level is, however, often sufficient to remove the ambiguity of the spin. Further information of a qualitative nature may be obtained from the intensity of the population of the levels. Information concerning the parities of levels may be inferred, in some cases, from the observation of pure multipole transitions.

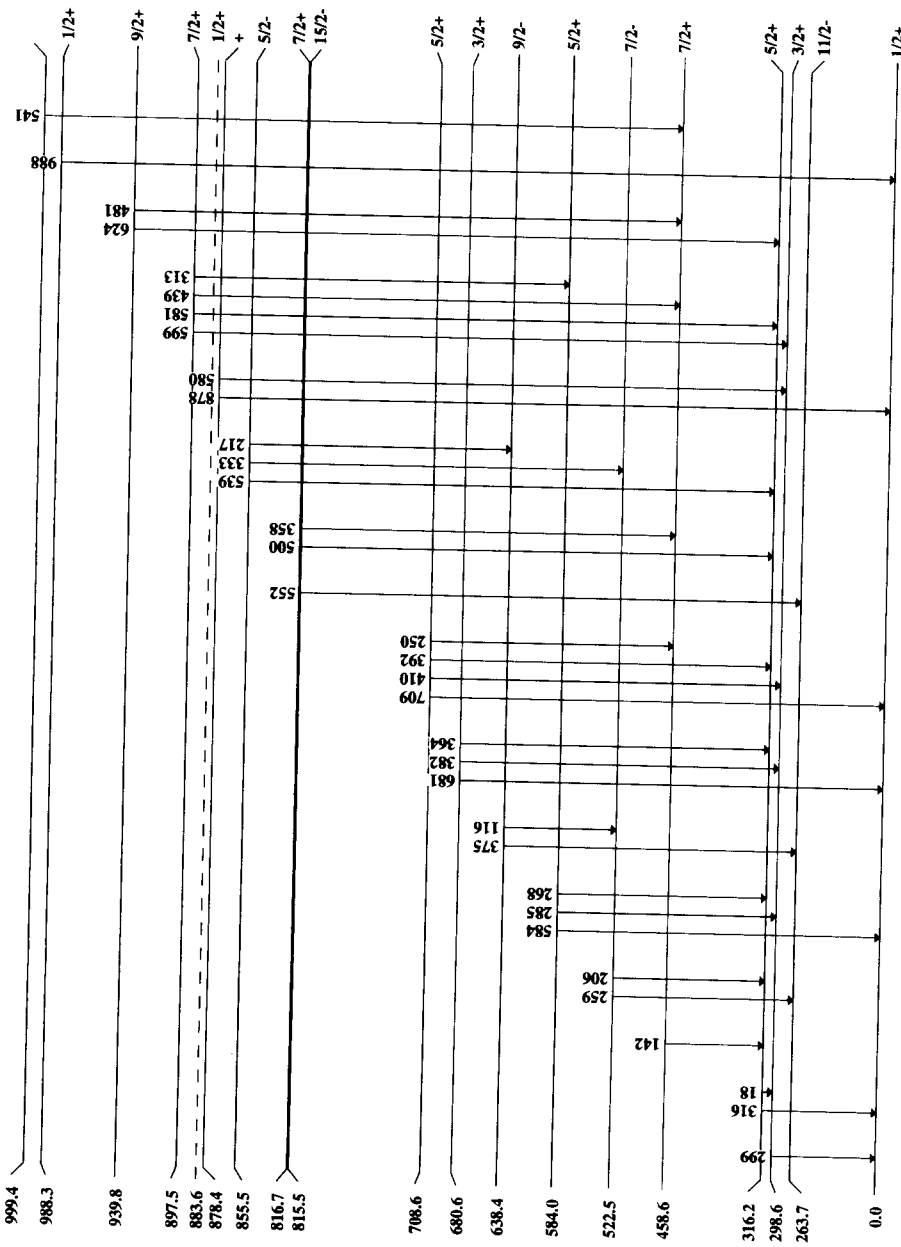

Fig. 5. Level scheme. Part I. Note that the energy scale is not linear. Note also that the 17.6 keV transition is inferred from coincidences and not observed. (For the 884 keV level, see comment in the text.)

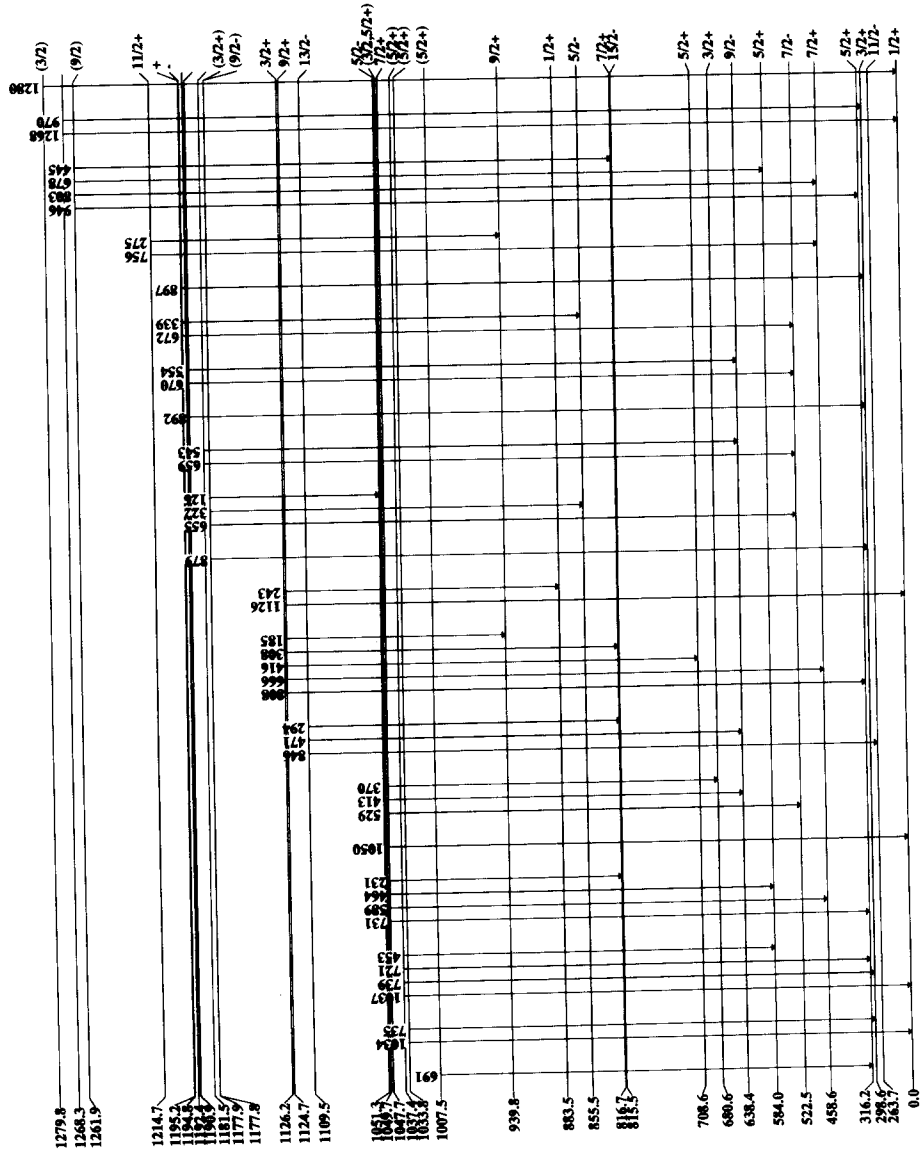

Fig. 6. Level scheme. Part II.

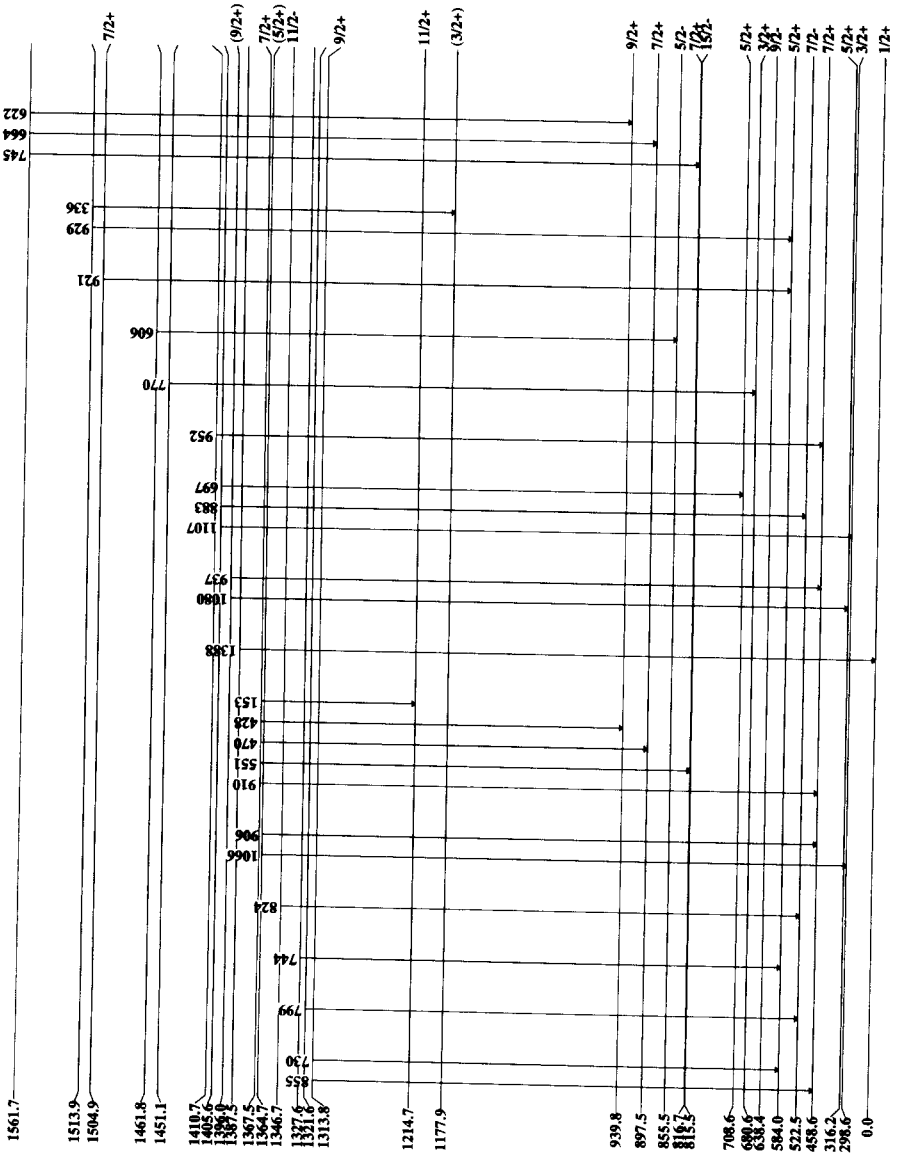

Fig. 7. Level scheme. Part III.

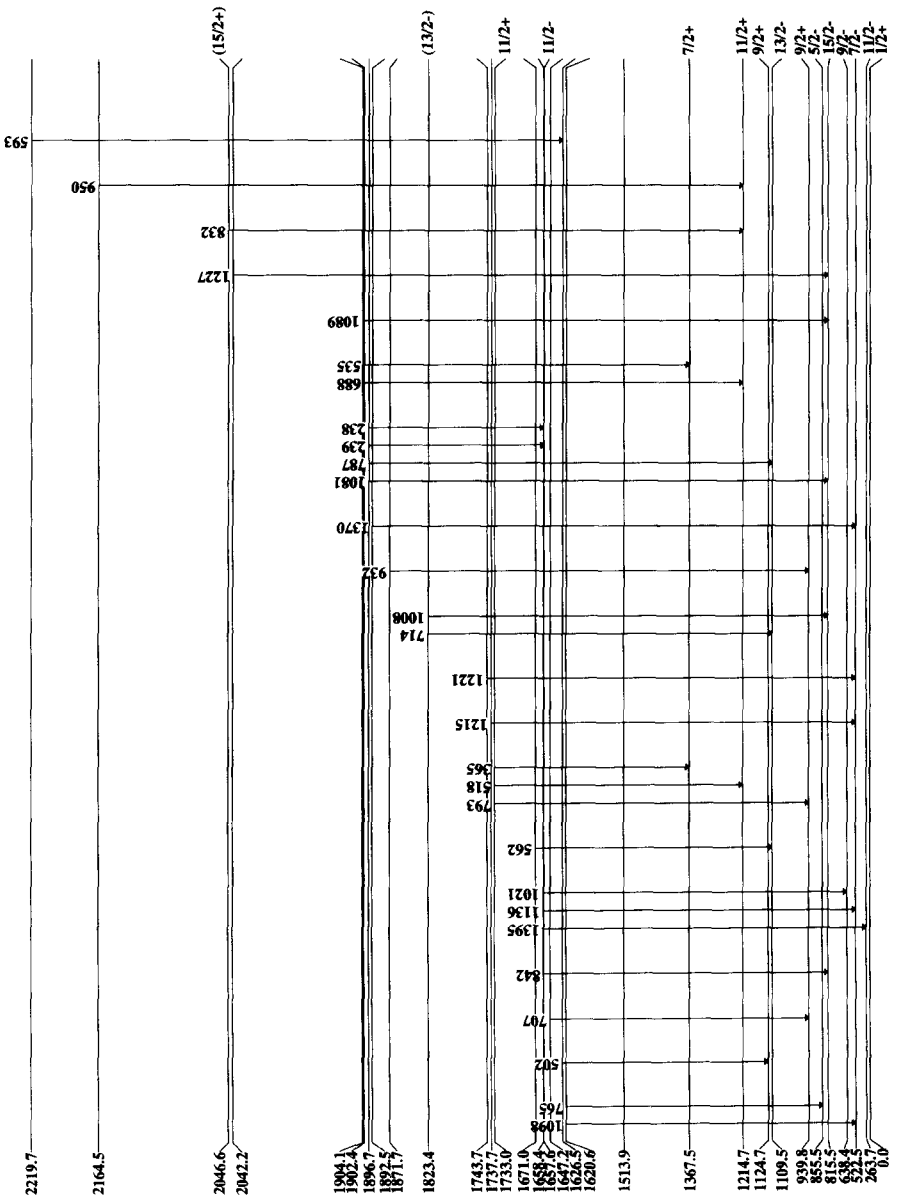

Fig. 8. Level scheme. Part IV.

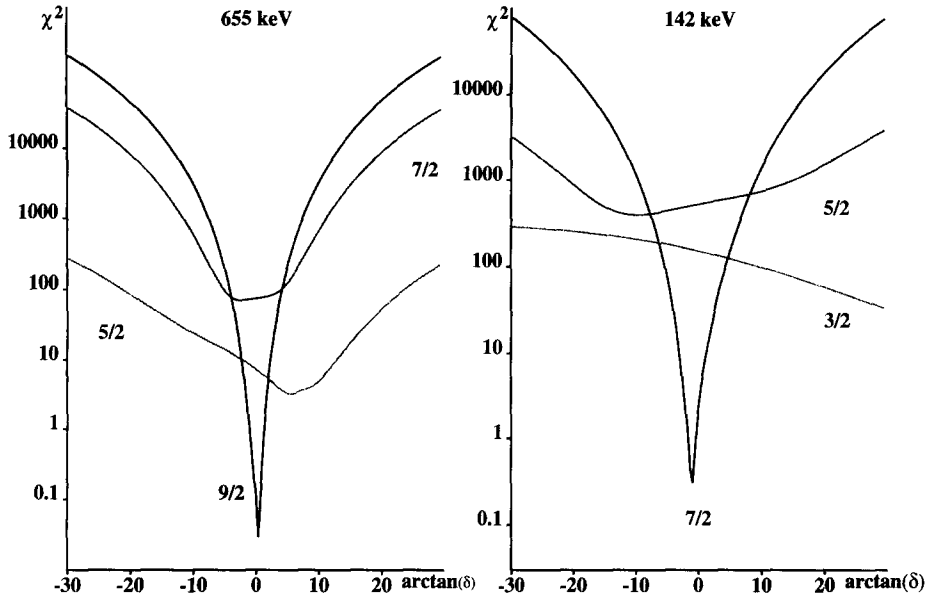

Fig. 9. Plots of χ^2 vs. arctan δ for selected γ-rays. For each plot three initial spin values were considered.

3.1.1. Angular distributions

In many cases it is only possible to determine whether a γ-ray is a pure or a mixed transition, which restricts the range of possible spins for the initial level, without yielding an unambiguous result. In cases where several γ-rays depopulate a single level, this ambiguity may often be removed when all the depopulating transitions are considered.

Where possible, the approach of Taras and Haas [7] and Ionescu et al. [8] has been adopted. The population of a given level is considered to be due to two mechanisms: (i) side-feeding, (ii) discrete transitions from other levels. The population of the magnetic substates is described by a Gaussian distribution due to side-feeding and a contribution from the discrete states which is treated by considering disorientation coefficients. The variance parameter σ of the side-feeding part was determined by considering pure E2 transitions and found to be 1.6(1). For mixed transitions, this parameter was used to perform the χ^2 analysis as a function of arctan δ and the initial spin, as reported in Ref. [8]. Table 1 summarises the values of δ wherever an unambiguous spin determination was possible. In some cases, two values of δ are possible for the same spin and both of these values are reported. Fig. 9 shows χ^2 plots as a function of arctan δ for two unambiguous cases.

3.1.2. Excitation function slopes

Following Ref. [6], the slope of the excitation function is defined as:

$$\mathrm{SL} = \frac{200}{E_2 - E_1}\left(\frac{I_2 - I_1}{I_2 + I_1}\right), \tag{1}$$

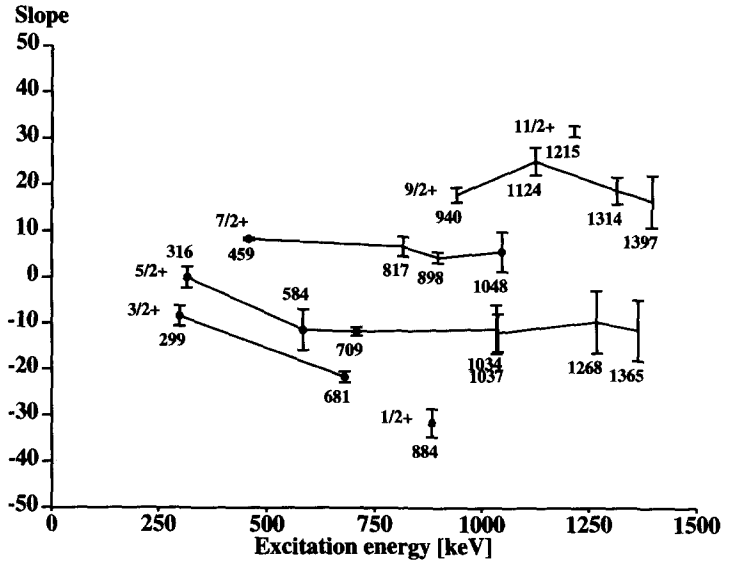

Fig. 10. Excitation function slopes as defined by Eq. (1). Data points denoted by full circles indicate that the spins were known previously.

where I_1 and I_2 are the γ-ray intensities measured at E_1 = 12.2 MeV and E_2 = 14.9 MeV, respectively. As can be seen from Fig. 10, the excitation function slopes of the depopulating transitions vary as a function of the excitation energy and spin of the initial level. Determination of the spin of the initial level for a γ-ray may be performed, in some cases, by comparing its slope to those of γ-rays depopulating levels of known spin.

The slopes of the excitation function are tabulated in Table 1. As can be seen from Table 3, by combination of the methods described above, a unique spin and parity has been assigned to most low energy (<1180 keV) levels. At higher excitation energy, the levels are only weakly populated by the (α,n) reaction making it difficult to assign spins.

4. Discussion of individual levels

In this section, the discussion is limited to those levels for which new information has been obtained or where disagreements with previous studies are found. Table 3 contains the full list of observed levels.

530(10) keV level: a level at 530(10) keV was observed in the (d,t) measurement of Goldman et al. [9], where the spin and parity were determined to be $\frac{7}{2}^+$ on the basis of L = 4 transfer. Such a level was not observed in the present work, but a $\frac{7}{2}^-$ level at 522.462(38) keV has been established. Inspection of Fig. 3 in the work of Goldman et al. [9] shows, however, that L = 3 transfer may not be ruled out for the level at 530(10) keV. It is assumed, therefore, that it has to be identified with the $\frac{7}{2}^-$ level at

Table 3
List of levels observed in the ^{110}Pd(α,nγ) reaction

Energy	Spin	Energy	Spin	Energy	Spin
0.0	$\frac{1}{2}^+$	1109.478(25)	$\frac{13}{2}^-$	1461.842(65)	
263.695(18)	$\frac{11}{2}^-$	1124.714(18)	$\frac{9}{2}^+$	1504.90(10)	$\frac{7}{2}^+$
298.604(14)	$\frac{3}{2}^+$	1126.221(47)	$\frac{3}{2}^+$	1513.944(69)	
316.224(14)	$\frac{5}{2}^+$	1177.79(30)	$(\frac{9}{2}^-)$	1561.675(21)	
458.634(23)	$\frac{7}{2}^+$	1177.850(36)	$(\frac{3}{2}^+)$	1620.575(42)	
522.462(38)	$\frac{7}{2}^-$	1181.535(28)		1626.481(22)	
583.976(15)	$\frac{5}{2}^+$	1190.85(13)		1647.214(44)	
638.408(61)	$\frac{9}{2}^-$	1192.35(11)		1657.566(38)	$\frac{11}{2}^-$
680.636(23)	$\frac{3}{2}^+$	1194.780(21)	$-$	1658.41(18)	
708.592(20)	$\frac{5}{2}^+$	1195.224(42)	$+$	1671.040(97)	
815.491(87)	$\frac{15}{2}^-$	1214.676(31)	$\frac{11}{2}^+$	1732.951(93)	$\frac{11}{2}^+$
816.723(25)	$\frac{7}{2}^+$	1261.883(95)	$(\frac{9}{2})$	1737.733(60)	
855.450(46)	$\frac{5}{2}^-$	1268.34(12)		1743.73(16)	
878.403(84)	$+$	1279.84(56)	$(\frac{3}{2})$	1823.393(30)	$(\frac{13}{2}^-)$
883.60(10)[a]	$\frac{1}{2}^+$	1313.761(19)	$\frac{9}{2}^+$	1871.65(26)	
897.536(18)	$\frac{7}{2}^+$	1321.604(78)		1892.540(54)	
939.772(20)	$\frac{9}{2}^+$	1327.60(44)		1896.664(73)	
988.294(29)	$\frac{1}{2}^+$	1346.731(30)	$\frac{11}{2}^-$	1902.360(33)	
999.416(63)		1364.700(64)	$(\frac{5}{2}^+)$	1904.118(83)	
1007.454(62)	$(\frac{5}{2}^+)$	1367.503(28)	$\frac{7}{2}^+$	2042.201(53)	
1033.800(23)	$(\frac{5}{2}^+)$	1387.495(40)		2046.60(15)	$(\frac{15}{2}^+)$
1037.416(71)	$(\frac{5}{2}^+)$	1395.97(38)	$(\frac{9}{2}^+)$	2164.50(12)	
1047.678(64)	$\frac{7}{2}^+$	1405.62(19)		2219.709(25)	
1049.739(95)	$(\frac{3}{2}, \frac{5}{2}^+)$	1410.670(53)			
1051.304(29)	$\frac{5}{2}^-$	1451.138(65)			

[a] Level energy and spin from literature [11]. This level probably exists, but is not observed in this work.

522.462(38) keV.

638.408(61) keV level: this level is well established and its existence is confirmed by this work. According to Baskova et al. [10] it decays by transitions of 322.35(3) and 374.64(3) keV. This decay mode is only partly confirmed, as the present data show that the placement of the 322.35(3) keV transition is incorrect. The coincidence data show clearly (see Table 2) that a 322.36(2) keV transition depopulates the 1177.79(30) keV level.

760(10) keV level: it has only been observed by Goldman et al. [9] who identified it as a $\frac{1}{2}^+$ state. The present data do not show any evidence for its existence, and although the (α,n) reaction only populates $\frac{1}{2}^+$ states weakly, on the basis of the excitation function trends, such a low-lying $\frac{1}{2}^+$ state should still be detectable.

883.60(10) keV level: this level has been reported in several works [11]. Its decay is reported to proceed via two transitions of 883.6(1) keV and 585(1) keV [12]. The placement of the 585(1) keV γ-ray was not confirmed in the (n, n$'\gamma$) measurements of Baskova et al. [10]. There is no evidence for such a level in this work. A transition of 583.97(1) keV was observed, but it is not in coincidence with the 298.60(1) keV transition and must be placed on the ground-state. An 883.43(4) keV transition was also observed; however, the coincidence relations show that it depopulates the 1405.62(19) keV level (see Table 2). Nevertheless, it is not possible to exclude the existence of a level at $\simeq$884 keV. If the level were (as reported by Goldman et al. [9]) a $\frac{1}{2}^+$ state, its population by the (α,n) reaction would be so weak that a ground-state transition would be masked by the observed 883.43(4) keV transition. As the level has been observed by several investigations (including (n,γ) measurements [10]), it is assumed that it most probably does exist. It is also noteworthy, that an intense 883.5 keV γ-ray is observed at a beam energy of 12 MeV. Most probably, this transition is not the same transition observed in the coincidence measurements at 16.2 MeV.

897.536(18) keV level: Goldman et al. [9] have observed a 900(10) keV level with $L = 2$ transfer. Based on cross-section ratios a spin of $(\frac{3}{2})^+$ was tentatively proposed. No γ decay is known for this level. In the present work, a level is observed at 897.536(18) keV. It decays by four transitions of 598.95(1), 581.26(9), 439.74(4) and 313.48(1) keV. On the basis of the angular distribution analysis, specifically for the 598.95(1) keV transition, a spin of $\frac{7}{2}^+$ is suggested. This is confirmed by the excitation function slopes, as can be seen from Fig. 10.

959.0(10) keV level: Goldman et al. [9] have observed a level at 960 keV. Baskova et al. [10] also observe a spin $\frac{5}{2}^+$ level at 959.0(10) keV depopulated by transitions of 643.14, 500.47(3) and 438.95(25) keV. The 643.14 keV transition is not observed in this work. A 500.50(1) keV transition is observed, but the coincidence relations do not corroborate the placement proposed by Baskova et al. [10] (see Table 2). The remaining transition, on the basis of the coincidence relations, populates the 458.634(23) keV level, rather than the 522.462(38) keV level suggested by Baskova et al. [10]. There is, therefore, no evidence for this level in the present study. It is noteworthy that in Fig. 1 of Goldman et al. [9], the peak corresponding to this level is labelled "0.96 imp", which seems to imply that it is due to an impurity. It is concluded that this level is spurious.

988.294(29) keV level: this level has been observed in various studies of ^{113}Cd [9,10,12]. Its depopulation has been established to be via transitions of 988.4(1) and 672.3(1) keV [12]. Baskova et al. [10] added two further depopulating transitions of 307.9(20) and 279.8(2) keV. The existence of this level and of the ground-state transition of 988.29(3) keV is confirmed by this work. However, the present coincidence relations show that the transition of 672.34(2) keV does not depopulate this level. The 307.89(2) keV transition, being in coincidence with the 500.50(1) keV transition (see Table 2), must also be placed elsewhere. The 279.8(2) keV transition observed by Baskova et al. [10] was not observed in the (α,nγ) experiments.

1177.79(30) and 1177.850(36) keV levels: Baskova et al. [10] observed a level at 1176.76(15) keV depopulated by a ground-state transition and a transition of 878.62(9) keV. In this work two levels at 1177.79(30) and 1177.850(36) keV are observed. According to the coincidence relations, the former decays via a 322.36(2) keV transition to the $\frac{5}{2}^-$ state at 855.450(46) keV, a 655.48(1) keV transition to the $\frac{7}{2}^-$ state at 522.462(38) keV and, a 126.48(1) keV transition to the $\frac{5}{2}^-$ state at 1051.304(29) keV. The angular distribution analysis of the 655.48(1) keV line (see Fig. 9) indicates that this transition depopulates a $\frac{9}{2}$ state. The 1177.850(36) keV level decays principally via an 879.2(3) keV to the $\frac{3}{2}^+$ state at 298.604(14) keV. This probably corresponds to the transition observed by Baskova et al., the difference in energy being attributed to the fact that there is a doublet at 878.4(2) and 879.2(3) keV. A transition from the 1177.850(36) keV level to the ground state can be neither confirmed nor denied on the basis of the $(\alpha,n\gamma)$ data. The decay mode of this level is therefore in accordance with the one proposed by Baskova et al. [10]. The spin differences rule out the possibility that the 1177.79(30) and the 1177.850(36) keV states are a single level.

5. Interpretation within the framework of the IBFM

In the IBFM, the odd-A nucleus is described by coupling an odd nucleon to the corresponding even–even core. In this calculation, an odd neutron is coupled to ^{112}Cd, which is described by the IBM-1. The odd neutron may occupy the $2d_{\frac{5}{2}}$, $1g_{\frac{7}{2}}$, $3s_{\frac{1}{2}}$ and $2d_{\frac{3}{2}}$ orbitals to produce positive-parity states and the $1h_{\frac{11}{2}}$ to produce negative-parity states.

The Hamiltonian H_B in the $U(5)$ dynamic symmetry limit is

$$H_B = \epsilon C_1(U(5)) + \alpha C_2(U(5)) + \beta C_2(O(5)) + \gamma C_2(O(3)). \tag{2}$$

The four parameters ϵ, α, β and γ have been determined by Délèze et al. [3] to be $\epsilon = 697.4$ keV, $\alpha \simeq 0$, $\beta = -9.8$ keV and $\gamma = 5.5$ keV. As these parameters provide a good description of the large number of experimentally known normal levels of ^{112}Cd, they were kept fixed in the present calculation. Note that the well-established intruder states in ^{112}Cd are not incorporated into the calculation. States produced by coupling an extra neutron to an intruder state will show up as extra experimental levels outside of the model space.

The odd neutron was described by a Hamiltonian H_F given by:

$$H_F = \sum_i E_i \hat{n}_i, \tag{3}$$

where E_i are the quasiparticle energies of the single-particle orbitals considered in the calculation and $\hat{n}_i$ yields the occupation of those orbitals.

Single-particle energies ϵ_i for the nearby tin isotopes, taken from Table 7 of Kuo et al. [13], were used to calculate the quasiparticle energies and the occupation probabilities v_i^2. A standard BCS calculation with a gap parameter $\Delta = 1.5$ MeV was performed

Table 4
Comparison of the single particle energies used in this calculation with those of Kuo et al. [7]. The deduced quasiparticle energies and occupation probabilities are also given. All energies are given in MeV

nlj	Single particle energies		$\|v_j\|^2$	Quasiparticle
	Ref. [13]	This work		energies
$1g_{7/2}$	0.00	−0.25	0.871	2.24
$2d_{5/2}$	0.00	0.00	0.843	2.06
$3s_{1/2}$	2.10	2.25	0.257	1.72
$1h_{11/2}$	3.60	2.85	0.155	2.08
$2d_{3/2}$	2.90	2.90	0.148	2.11

and the values of Kuo et al. were then adjusted to fit the experimental energies. Apart from the $1h_{\frac{11}{2}}$ single-particle energy, which needed to be lowered considerably, there is little change. This can be seen from Table 4 which compares the ϵ_i values used in this calculation and those of Kuo et al. and also reports the calculated E_i and v_i^2 values. A similar value for the $1h_{\frac{11}{2}}$ orbit was also needed in the calculation of Donau and Hageman for ^{107}Cd [14].

A third term V_{BF} is required to describe the boson–fermion interaction. This consists of a monopole, a quadrupole and an exchange force term. Scholten has shown [15] that these terms are:

$$V_{BF} = \sum_j A_j \hat{n}_d \hat{n}_j + \sum_{jj'} \Gamma_{jj'} (Q_B^{(2)} \cdot (a_j^\dagger \tilde{a}_{j'})^{(2)}) + \sum_{jj'j''} \Lambda_{jj'}^{j''} : ((d^\dagger \tilde{a}_j)^{(j'')} \times (\tilde{d} a_{j'}^\dagger)^{(j'')})_0^{(0)} : , \tag{4}$$

with

$$Q_B^{(2)} = (s^\dagger \tilde{d} + d^\dagger s)^{(2)} + \chi (d^\dagger \tilde{d})^{(2)}, \tag{5}$$

and $\hat{n}_d$ the d-boson number operator.

Semi-microscopic arguments based on the underlying quasiparticle structure of the odd neutron are used to reduce the model space leading to the following expressions: [15]

$$\Gamma_{jj'} = \Gamma_0 (u_j u_{j'} - v_j v_{j'}) Q_{jj'}, \tag{6}$$

$$\Lambda_{jj'}^{j''} = \frac{-2\sqrt{5}\Lambda_0 \beta_{jj''} \beta_{j''j'}}{\sqrt{2j''+1}\,(E_j + E_{j''} - \hbar\omega)}, \tag{7}$$

$$\beta_{jj'} = (u_j v_{j'} + v_j u_{j'}) Q_{jj'}, \tag{8}$$

where $Q_{jj'}$ is defined as $\langle j||Y_2||j'\rangle$, and v_j^2 are the occupation probabilities ($u_j^2 = 1 - v_j^2$) given in Table 4. The $(E_j + E_{j''} - \hbar\omega)$ term in (Eq. (7)) takes into account the energy difference between the fermion single-particle orbitals and a D-fermion pair [15]. By considering the excitation energies of the 2_1^+ states in the even tin nuclei, the value

of $\hbar\omega$, which denotes the energy difference between the D- and S- fermion pairs, was found to be 1.5 MeV.

The total Hamiltonian used to describe the odd-A nucleus is the sum of these three terms:

$$H = H_B + H_F + V_{BF}. \tag{9}$$

It was diagonalised numerically using the computer code ODDA [16].

5.1. Positive-parity states

Only four parameters remained free in the calculation for ^{113}Cd, and, by fitting the observed positive-parity states, they were found to be $A_i = -0.15$, $\Gamma_0 = 0.2$, $\Lambda_0 = 2.2$, $\chi = -0.1$. These four parameters represent, respectively, the monopole strength, the quadrupole strength , the exchange force strength and the χ term in the quadrupole operator (Eq. (5)). These values not only reproduce reasonably well the observed levels of ^{113}Cd, but it has been checked that similar parameters may also be used to describe ^{111}Cd. Fig. 11 compares the positive-parity states of the experimental spectrum with those of the IBFM calculation.

5.2. Negative-parity states

The same set of parameters used for the calculation of the positive-parity states, when applied to the negative-parity states, did not reproduce the experimental spectrum as can be seen from the calculation TH1 in Fig. 11. In particular, this calculation predicts a set of five weakly coupled states at just under 1 MeV, which is not observed experimentally.

There are two ways in which one can resolve a problem of this type: either different Hamiltonians can be used to describe the positive- and negative-parity states, or the model space can be enlarged. The former approach is widely used; however, it is to a certain extent in contradiction with the use of the parametrisation described above.

If a value of $\chi = -2.5$ was adopted and the other parameters refitted, the calculation, shown as TH2 in Fig. 11, gave a crude reproduction of the experimental level scheme. The calculated spectrum is far from acceptable, however, as the weakly coupled quintuplet at around 1 MeV remains, albeit with a slightly larger spacing between the states. Such a large value of χ for negative-parity states but not for positive ones, is very unlikely to be due to a physical phenomenon and must be attributed to what Lipas describes as "misuse of the IBM" [17]. It was therefore necessary to look for an alternative solution. The observation of a large number of low-spin negative-parity states at low excitation energies, observed in single particle transfer reactions [18], indicates that considering only the unique parity orbital is too restrictive. It is therefore necessary to enlarge the model space by including additional single particle orbitals in the calculation.

A significant piece of information is given by the fact that the second negative-parity state, i.e. the $\frac{7}{2}^-$, is considerably lower than the first calculation would imply. This leads

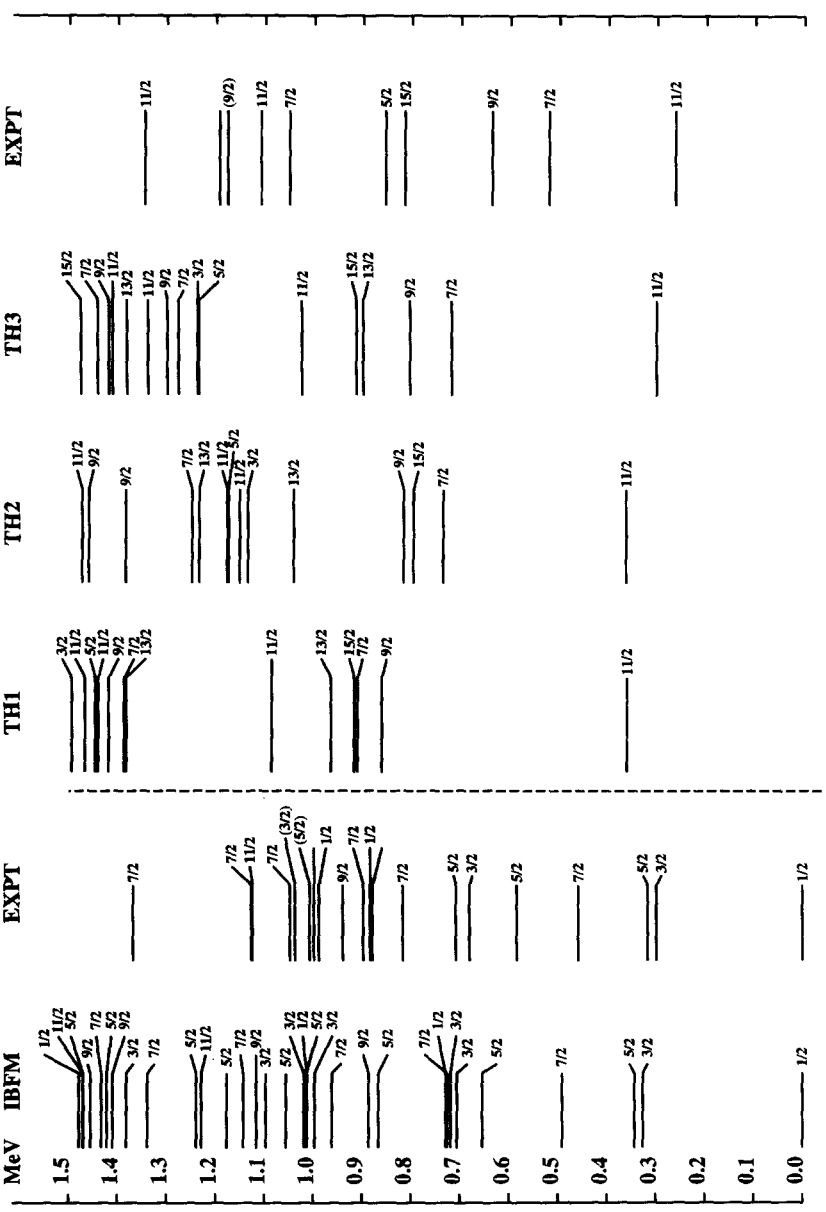

Fig. 11. Comparison between the IBFM and experiment. The column labelled IBFM shows the calculation for positive-parity states, compared with the experimentally observed states in column 2. TH1, TH2 and TH3 are the three negative-parity calculations described in the text compared with the experimental results in the last column.

one to suspect that the $2f_{\frac{7}{2}}$ orbital may be playing an important rôle. Including this orbital in the calculation tends to lower the $\frac{7}{2}^-$ state dramatically whilst having little effect on the higher spin states. It was found that by considering both the $1h_{\frac{11}{2}}$ and the $2f_{\frac{7}{2}}$ single-particle orbitals, it was possible to reproduce the experimental spectrum using the same boson–fermion interaction parameters as for the positive-parity states. For this orbital a quasiparticle energy of $E_{f_{\frac{7}{2}}} = 3.5$ MeV with an occupation probability of $v_{f_{\frac{7}{2}}} = 0.05$ was used for the calculation, shown in Fig. 11 as TH3. As in the $h_{\frac{11}{2}}$ orbit case, this quasi-particle energy corresponds to a lowering of the single particle energy by 1 MeV. The contribution of the $2f_{\frac{7}{2}}$ orbit in the wave-function of the lowest excited states is of the order of 10% for the low-spin states and reduces to about 3% for states having a spin larger than $\frac{7}{2}$. In view of this it would be of interest to extend the experimental knowledge of the level scheme to higher spin values. To test the $f_{\frac{7}{2}}$ contribution to the wave-functions transfer reactions could provide a more stringent test. According to Németh et al. [18] there seems to be indication of $f_{\frac{7}{2}}$ strength in the first excited $\frac{7}{2}^-$ state in Pd and Cd isotopes.

Another interesting feature of this calculation is that it also reproduces nicely the excitation energy of the lowest $\frac{11}{2}^-$ state with respect to the ground state (see Fig. 11). This is comforting in view of the need to reduce the single particle energies of both negative-parity orbitals by 1 MeV.

5.3. States coupled to intruder states in the even–even core

In view of the presence of low-lying intruder states in ^{112}Cd [2], one would also expect the coupling of an extra neutron to these states to produce additional levels in ^{113}Cd outside of the model space of these calculations. However, the only candidate for such a state observed in this work is the level at 1049.7 keV, suggested by Németh et al. [18] to have $I^\pi = \frac{1}{2}^+$. Although it lies at an energy expected for an intruder state, this clearly does not constitute sound evidence that it indeed has an intruder configuration. Furthermore, the present data favour a spin of $\frac{3}{2}$ or $\frac{5}{2}$. The evidence for intruder states in ^{113}Cd is therefore insufficient. In order to search for such states it is necessary to perform more experiments, in particular measurements using the (n,n′γ) reaction which can populate low-spin states far above the yrast line, contrary to the (α,n) reaction.More data on the electromagnetic properties including lifetimes are also required.

A moot point is the influence of the mixing between normal and intruder states in the core. Following Jolie and Lehmann [19] this mixing should be very weak except for the two phonon 0^+ state. With the present level of experimental knowledge of the odd-mass Cd isotopes, the identification of states based on mixed core-states seems even more difficult than the identification of additional states.

6. Conclusion

The present study has, using the $(\alpha,n\gamma)$ reaction, extended the level scheme of ^{113}Cd, especially for the higher-spin and negative-parity states. Spins were assigned to a large fraction of the levels, but further studies are required, especially to observe higher spin states and assign unique spins and parities to levels above 1180 keV excitation energy.

The IBFM has been demonstrated to describe the positive-parity states rather well, however, the description of the negative-parity states is somewhat poorer. This may be due to the limited knowledge of the spins of the negative-parity states. Substantial improvement was obtained with the inclusion of the $2f_{\frac{7}{2}}$ orbital, which made it possible to use the same hamiltonian to describe both positive and negative-parity states.

Acknowledgements

The authors would like to thank Drs. Stammbach and Schmelzbach and the PSI cyclotron crew, for the preparation of the α beams. Financial support for P.E.G. was provided in part by the U.S. National Science Foundation under grant PHY-9300077.

References

[1] R.A. Ward, Astron. Astrophys. 103 (1981) 189.
[2] M. Délèze, S. Drissi, J. Kern, P.A. Tercier, J.-P. Vorlet, J. Rikovska, T. Otsuka, S. Judge and A. Williams, Nucl. Phys. A 551 (1993) 269.
[3] M. Délèze, S. Drissi, J. Jolie, J. Kern and J.P. Vorlet, Nucl. Phys. A 554 (1993) 1.
[4] J.L. Wood, K. Heyde, W. Nazarewicz, M. Huyse and P. Van Duppen, Phys. Rev. 215 (1992) 101.
[5] V.A. Ionescu, J. Kern, C. Nordmann, S. Olbrich and Ch. Rhême, Nucl. Instr. and Meth. 163 (1979) 395.
[6] J. Kern, A. Bruder, S. Drissi, V.A. Ionescu and D. Kusnezov, Nucl. Phys. A 512 (1990) 1.
[7] P. Taras and B. Haas, Nucl. Instr. and Meth. 123 (1975) 73.
[8] V.A. Ionescu, J. Kern, C. Nordmann, S. Olbrich and W. Reichart, Nucl. Instr. and Meth. 190 (1981) 19.
[9] L.H. Goldman, J. Kremnek and S. Hinds, Phys. Rev. 179 (1969) 1172.
[10] K.A. Baskova, A.B. Vovk, T.M. Gerus, L.I. Gorov, A.M. Demidov, V.A. Kurkin, IAE 4544/2 (1987).
[11] J. Lyttkens, K. Nilson and L.P. Ekström, Nuclear data sheets 33(1) (1981) 1.
[12] J. Lyttkens, K. Nilson and L.P. Ekström, Nuclear data sheets 33(1) (1981) 1; referring to J. Phys. Soc. Jpn. 44 (1978) 1062.
[13] T.T.S. Kuo, E. Baranger, M. Baranger, Nucl. Phys. 81 (1966) 241.
[14] F. Donau and U. Hageman, Nucl. Phys. A 256 (1976) 27.
[15] O. Scholten, Ph.D. thesis, University of Groningen, The Netherlands (1980), unpublished.
[16] O. Scholten, program package ODDA, KVI internal report, no. 255 (1980).
[17] P.O. Lipas, 8th Int. Symp. on Capture Gamma-Ray Spectroscopy and Related Topics, Fribourg, Switzerland, 1993, ed. J. Kern (World Scientific, Singapore, 1994) p. 177.
[18] Zs. Németh et al., 8th Int. Symp. on capture Gamma-Ray Spectroscopy and Related Topics, Fribourg, Switzerland, 1993, ed. J. Kern (World Scientific, Singapore, 1994) p. 314.
[19] J. Jolie and H. Lehmann, Phys. Lett. B 342 (1995) 1.